

# One-step synthesis of flower-like $\eta$ -Al<sub>2</sub>O<sub>3</sub> via supercritical hydrothermal method

Behrouz Jalouli<sup>1</sup>, Aref Abbasi<sup>2</sup>, Seyed Mohammad Musavi Khoei<sup>1</sup> ✉

<sup>1</sup>Department of Mining and Metallurgy, Amirkabir University of Technology, Tehran, Iran

<sup>2</sup>School of Metallurgy and Materials Engineering, Iran University of Science and Technology (IUST), Narmak, Tehran, Iran

✉ E-mail: mmousavi@aut.ac.ir

Published in Micro & Nano Letters; Received on 18th April 2020; Revised on 30th July 2020; Accepted on 25th August 2020

In this Letter, flower-like  $\eta$ -Al<sub>2</sub>O<sub>3</sub> nanostructure was synthesised via hydrothermal method without any surfactant or further calcination. A molten salt bath rose the reactor temperature as much as 500°C to achieve the supercritical condition. Such a high temperature caused a rapid one-step synthesis in two minutes. Al(NO<sub>3</sub>)<sub>3</sub> and NaOH were the only precursors. Synthesised powders were investigated by X-ray powder diffraction and scanning electron microscope, and the specific surface area was also determined by N<sub>2</sub> adsorption–desorption analysis. Increasing reaction time >2 min caused undesired Ostwald ripening. So instead of giving more time, a small amount of NaOH was added to form the  $\eta$ -Al<sub>2</sub>O<sub>3</sub> phase. Moreover, the morphology of  $\eta$ -Al<sub>2</sub>O<sub>3</sub> changed to flower-like by increasing the density of the supercritical fluid. Finally, the probable mechanism of flower-like morphology formation was proposed in two steps.

**1. Introduction:** Alumina exists in several polymorphs, including  $\alpha$ ,  $\gamma$ ,  $\delta/\theta$  and  $\eta$  [1, 2]. This polymorphism can be useful in various applications such as water treatment, gas adsorption, catalysts etc. [3–14].

It has been found that alumina phases transform to each other over the temperature changes [15, 16]. These transformations happen in a sequence of  $\gamma/\alpha$ -Al(OH)<sub>3</sub> to  $\rho$ -Al<sub>2</sub>O<sub>3</sub> and  $\rho$ -Al<sub>2</sub>O<sub>3</sub> to  $\eta/\gamma$ -Al<sub>2</sub>O<sub>3</sub> and finally all of these metastable phases irreversibly transform to the stable  $\alpha$ -Al<sub>2</sub>O<sub>3</sub> at around 1050°C [17].

Except  $\alpha$ -Al<sub>2</sub>O<sub>3</sub>, the other metastable phases can be used as catalyst support [18–30]. Between various phases of alumina,  $\gamma$  and  $\eta$ -Al<sub>2</sub>O<sub>3</sub>, with similar structures, have been widely employed as catalysts or catalyst support in the Fischer–Tropsch process, hydrocracking and so on [31–33]. Compared with  $\gamma$ -Al<sub>2</sub>O<sub>3</sub>,  $\eta$ -Al<sub>2</sub>O<sub>3</sub> has higher activity due to its lower surface energy and higher specific surface area, which is proper for catalytic applications [34, 35].

Owing to its lower surface energy,  $\eta$ -Al<sub>2</sub>O<sub>3</sub> becomes more stable by the reduction of particle size rather than the other polymorphs. Moreover, it is stable over the temperature range at which most of the catalytic reactions take place.

To achieve the maximum reachable active surface, we have to produce anisotropic nanostructures by manipulating the morphology of the synthesised phases. In this regard, mass production of  $\eta$ -Al<sub>2</sub>O<sub>3</sub> nanostructures with needed size and morphology is highly requested, since each morphology exhibit properties which are desired for a particular application. Between the well-known morphologies (i.e. spherical, cubic, rod, wire, tube, plate-like, flake, film, polyhedral and so on), hierarchical flower-like structures present an outstanding active surface area which is proper for catalysts.

Despite having these advantages, not much attention has been paid to the  $\eta$ -Al<sub>2</sub>O<sub>3</sub> synthesis. Pradhan *et al.* [36] synthesised  $\eta$ -Al<sub>2</sub>O<sub>3</sub> via a wet chemical route. They produced  $\eta$ -Al<sub>2</sub>O<sub>3</sub> by calcination of basic aluminium sulfate at 900°C. In another research,  $\eta$ -Al<sub>2</sub>O<sub>3</sub> was produced by calcination bayerite ( $\gamma$ -Al(OH)<sub>3</sub>), which had been formed from the hydrolysis of NaAlO<sub>2</sub> solution [34]. Seo *et al.* prepared  $\eta$ -Al<sub>2</sub>O<sub>3</sub> using a two-step approach, i.e. sol–gel preparation by aluminium-tri-sec-butoxide, then calcination at 300–700°C [37]. Osman *et al.* [25, 26, 38] reported  $\eta$ -Al<sub>2</sub>O<sub>3</sub> synthesis via precipitation of Al(NO<sub>3</sub>)<sub>3</sub> and AlCl<sub>3</sub> solutions by ammonia followed by calcination and obtained precipitates at 300–550°C.

In all previous researches,  $\eta$ -Al<sub>2</sub>O<sub>3</sub> has been synthesised by a two-step approach, including AlOOH synthesis and calcination. As this calcination is carried out in a temperature range of 400–700°C, and because of the long time that it takes, synthesis procedures usually take too much time and energy, which makes them unprofitable for industrial scale-up.

Herein, for the first time, a rapid one-step high temperature supercritical hydrothermal synthesis of Al<sub>2</sub>O<sub>3</sub> without calcination has been reported. In this work, flower-like  $\eta$ -Al<sub>2</sub>O<sub>3</sub> nanostructure was produced in 2 min by tuning the synthesis parameters such as time, NaOH and supercritical solution density at 500°C.

## 2. Materials and methods

**2.1. Reactor:** A double-layered reactor chamber (Fig. 1a) was designed and manufactured with a capacity of 24 ml. The outer layer was made of hardened hot work steel (AISI H13), which is a heat and thermal shock resistant steel, and the inner layer was made of corrosion-resistant stainless steel AISI 316L. The reactor's opening cap was sealed with a carbon heat resistant sealant. This set up with a safety factor of 4 was prepared to endure 600°C temperature and 60 MPa pressure. In order to prohibit heterogeneous nucleation and growth, the surface of the inner layer was polished to reach a mirror-like surface (Fig. 1b).

**2.2. Synthesis procedure:** The adequate amounts of Al(NO<sub>3</sub>)<sub>3</sub> and NaOH (both were obtained from Merck, Germany) were dissolved in deionised water. Then, a specific volume of solution was charged into the carbon sealed reactor. The reactor was subsequently entered into the molten inert salt bath to be heated at desired temperatures, according to Table 1. After spending favourable time, the reactor was immediately quenched in cold water in order to prevent the reaction from advancing and to achieve the appropriate product.

Various experiments were carried out in this research for investigating different parameters' effects on the shape, particle size and synthesised phases. These factors included reaction time, NaOH concentrations and precursor solution volume, which are shown in Table 1.

**2.3. Characterisation:** Morphological investigations were carried out by the scanning electron microscope (SEM, XL30, Philips, Netherlands) and (SEM, AIS2100, Seron Technology, South Korea). The phases of synthesised powders were identified by

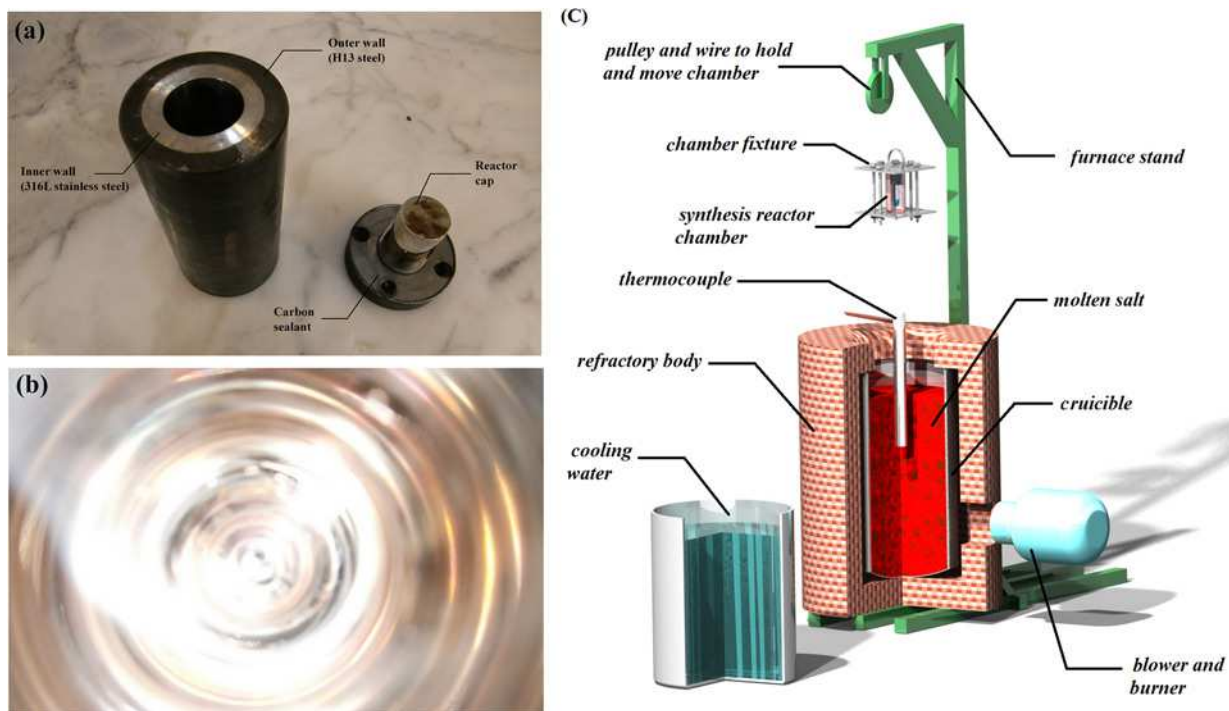


**Fig. 1** Synthesis setup  
 a Synthesis reactor  
 b Mirror-like inner surface of the reactor  
 c Schematic representation of the furnace, molten salt and quench water bath

**Table 1** Nomenclature of samples and their synthesis conditions

Sample code	Time, min	[NaOH], mol/l	Density*, g/cm <sup>3</sup>	Alumina, %
1	2	0	0.17	0
2	3	0	0.17	0
3	4	0	0.17	0
4	15	0	0.17	14
5	2	0.3	0.17	23
6	2	0.6	0.17	53
7	2	0.6	0.25	71
8	2	0.6	0.34	84

\*Supercritical fluid density.

X-ray diffraction (XRD, Equinox 3000, INEL company, France) with Cu K $\alpha$  ( $\lambda=0.15418$  nm) radiation. The pH of precursor solutions was measured by a pH meter (pH50+DHS, X.S. instruments, Italy). The specific surface area of the obtained  $\eta$ -Al<sub>2</sub>O<sub>3</sub> powder was determined using adsorption and desorption of Nitrogen (BET, 3P micro 200, 3P Instruments, Germany).

### 3. Results and discussion

3.1. Appropriate time: Huge reaction rate makes the supercritical hydrothermal synthesis 1000 times faster than conventional hydrothermal one [39]. Owing to the high pressure and temperature, the supercritical hydrothermal condition has become an advantageous approach to the synthesis of high crystalline metal oxide compounds [40–42]. Time dependency of the particle morphology and phase were evaluated at various times. Fig. 2 shows the SEM micrograph of particles obtained from different reaction times (2, 3, 4 and 15 min). With an increase in reaction time, Ostwald ripening can be observed as a result of the time-dependent diffusive nature of this phenomenon. As this Figure shows, big particles cannibalised small ones, so that particle size distribution became

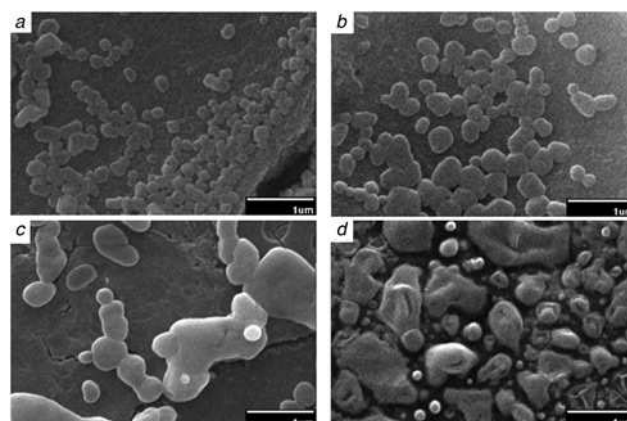


**Fig. 2** SEM images of samples which show the reaction time effect on particle growth  
 a Sample 1 synthesised in 2 min  
 b Sample 2 synthesised in 3 min  
 c Sample 3 synthesised in 4 min  
 d Sample 4 synthesised in 15 min

non-uniform. In 2 min, reaction time (Fig. 2a), there was not sufficient time for mass transfer, and particle sizes have not been influenced by Ostwald ripening.

Noguchi *et al.* [43] explained the supercritical hydrothermal reaction mechanism of Al<sub>2</sub>O<sub>3</sub> in three different steps as follows:

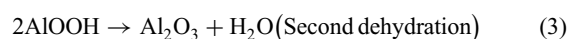
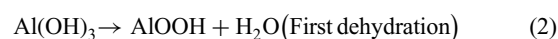
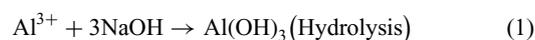
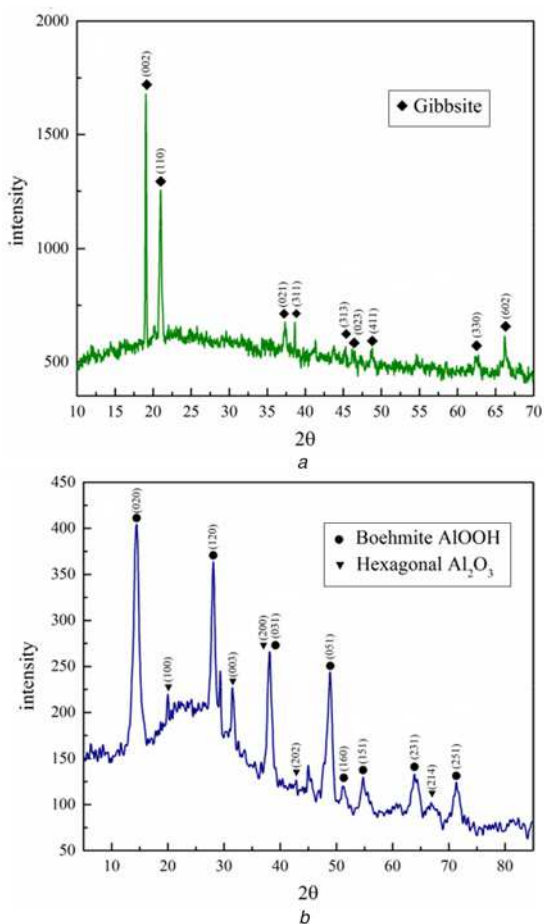


Fig. 3a shows the XRD pattern of sample 1 at 500°C and 2 min of reaction time without the presence of NaOH. The pattern indicates



**Fig. 3** XRD patterns of samples at different synthesis condition  
 a Sample 1 synthesised in 2 min  
 b Sample 4 synthesised in 15 min

that in this condition, only the hydrolysis reaction (1) occurred, and Gibbsite ( $\text{Al}(\text{OH})_3$ ) was the only product. A comparison between samples 1 and 4 (Figs. 3a and b) gives us a clue that raising the reaction time from 2 to 15 min at  $500^\circ\text{C}$  causes the first dehydration reaction (2) to be completed by producing Boehmite.

To reach a desirable phase and morphology, proper time and temperature should be considered for the synthesis. Conventional hydrothermal synthesis carries out in a wide range of temperatures from  $100^\circ\text{C}$  up to the critical temperature of water ( $374^\circ\text{C}$ ). Also, in supercritical synthesis, the temperature is set to near the critical temperature (e.g.  $400^\circ\text{C}$ ). In the continuous supercritical synthesis method, the reaction occurs at a fraction of a second while in supercritical batch, the reaction takes 10 min to a couple of hours to proceed at the range of critical temperature. For achieving the  $\eta\text{-Al}_2\text{O}_3$  phase, the experiments were carried out at  $500^\circ\text{C}$  in this research. Owing to the increase in high temperature, nucleation and growth rates the precipitate formation is accelerated [44]. As it was discussed before, the increased time caused particles' secondary growth at high temperature. To eliminate undesired Ostwald ripening, a molten salt bath was used as a rapid heating source to speed up the reaction and finish it before secondary growth. Therefore, the experiments were performed in 2 min to prohibit Ostwald ripening. However, this time is not sufficient for boehmite or  $\text{Al}_2\text{O}_3$  formation at  $500^\circ\text{C}$ . Thus, another remedy should be investigated to achieve these phases.

**3.2. Synthesis  $\eta\text{-Al}_2\text{O}_3$ :** Mineraliser is an important factor in inorganic hydrothermal synthesis. Hydroxides, halides, sulfides, carbonates etc. can be used as a mineraliser. Hydroxide is one of

the most effective anions in oxides synthesis in the precursor solution [45]. The solubility of the amphoteric species (such as aluminium oxide) is related to the mineraliser concentration [46]. Thus, in this research, the concentration of soluble Al-compounds was raised by adding NaOH. Besides, adding more  $\text{OH}^-$  as one of the reactants in  $\text{Al}_2\text{O}_3$  formation – causes the system to form more of it.

According to the XRD pattern of sample 6 ( $\text{pH}=11$ ), which is shown in Fig. 4, increasing in precursor solution pH resulted in Diaspore ( $\text{AlOOH}$ ) and  $\eta\text{-Al}_2\text{O}_3$  formation.

The effect of NaOH concentration on the morphology of the particles is illustrated in Fig. 5. In these samples, NaOH increases from left to right. By increasing NaOH concentration, spherical particles transformed to plate ones. Further increase in NaOH concentration causes monomer concentration rise, which resulted in flake-like particles formation.

**3.3. Synthesis of flower-like  $\eta\text{-Al}_2\text{O}_3$ :** Another important factor in the supercritical state that affects morphology, is the supercritical fluid density. So, without making any changes in concentration, time or temperature, this factor was investigated for further morphological clarifications. As a consequence of liquid expansion, the final supercritical fluid volume is equal to the reactor volume.

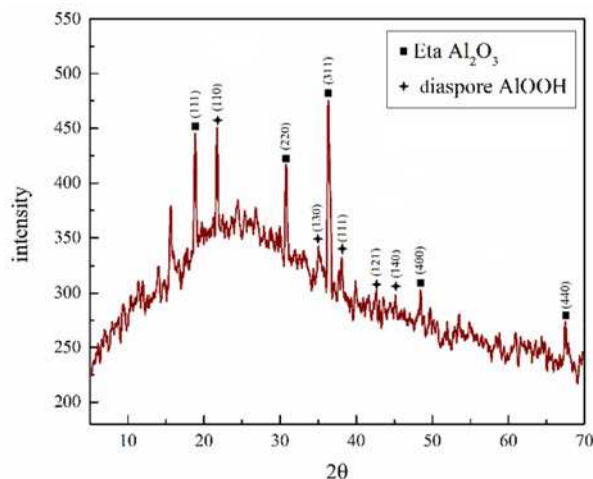


**Fig. 4** XRD patterns of sample 6:  $500^\circ\text{C}$ , 2 min,  $[\text{NaOH}] = 0.6 \text{ M}$ , supercritical fluid density =  $0.17 \text{ g/cm}^3$  (JCPDS file numbers of  $\eta\text{-Al}_2\text{O}_3$  and diaspore are 00-047-1292 and 00-081-0465, respectively)

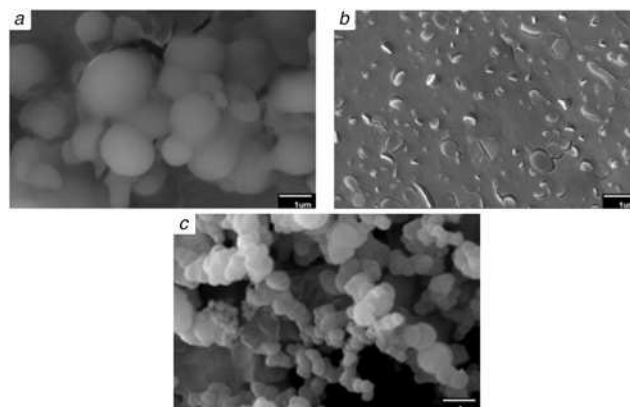


**Fig. 5** SEM micrographs of  
 a Sample 1- $[\text{NaOH}]=0$   
 b Sample 5- $[\text{NaOH}]=0.3$   
 c Sample 6- $[\text{NaOH}]=0.6$

Since the reactor volume is constant, increasing the precursor solution volume raises the supercritical fluid density (4)

$$\text{Supercritical fluid density} = \frac{\text{Precursor mass}}{\text{Reactor volume}} \quad (4)$$

According to Figs. 6a–c, the supercritical fluid density increased from 0.17 to 0.25 and 0.34 g/cm<sup>3</sup>, respectively which led to a morphology trend from circular nanoflake to agglomerated particle and finally to the flower-like hierarchical structure at 0.34 g/cm<sup>3</sup>. Increasing the density from 0.17 to 0.34 g/cm<sup>3</sup> caused Diaspore amount to decrease and η-Al<sub>2</sub>O<sub>3</sub> became the predominant produced phase (Fig. 7).

The surface area of the product was also determined by N<sub>2</sub> adsorption–desorption analysis. The result in Fig. 8 shows that the Al<sub>2</sub>O<sub>3</sub> affords a high surface area of 106.7 m<sup>2</sup>/g.

The yield of reactions measured by the weight loss in calcination at 900°C, and data was added to Table 1. Increasing time, NaOH concentration and supercritical fluid density caused dehydration reactions (2) and (3) advancement.

3.4. Suggested mechanism for flower-like η-alumina: As a result of doubling the solution density from 0.17 (sample 6) to 0.34 g/cm<sup>3</sup> (sample 8), monomer concentration doubled, and the supersaturation increased significantly. In this condition, it was observed that a huge number of plates emerged rapidly from a single spot and formed particles with a hierarchical structure. If the driving force rises so much, due to the radial growth from the centre, hierarchical

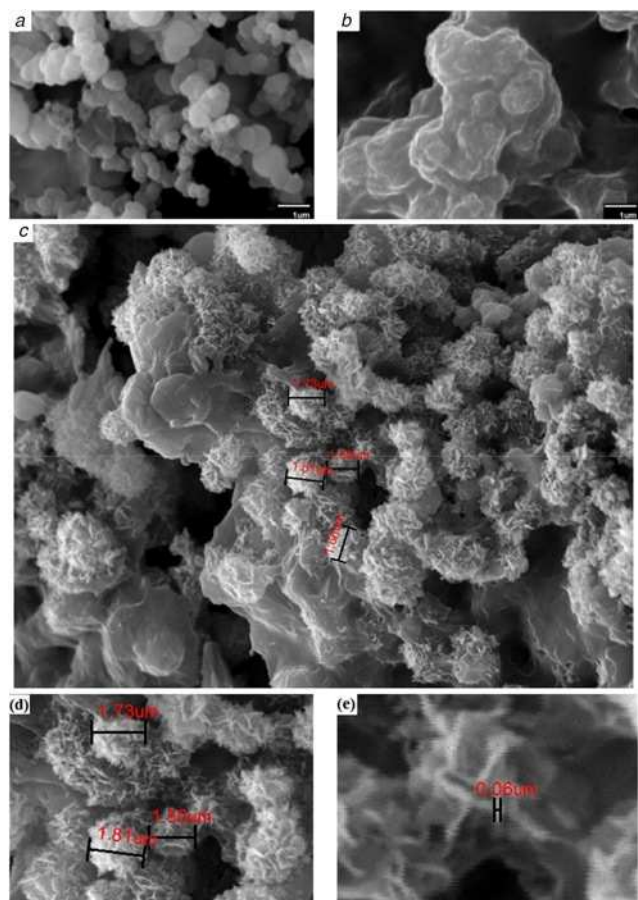


**Fig. 6** SEM micrographs of  
a Sample 6 with 0.17 g/cm<sup>3</sup> supercritical fluid density  
b Sample 7 with 0.25 g/cm<sup>3</sup> supercritical fluid density  
c–e Sample 8 with 0.34 g/cm<sup>3</sup> supercritical fluid density in different magnifications

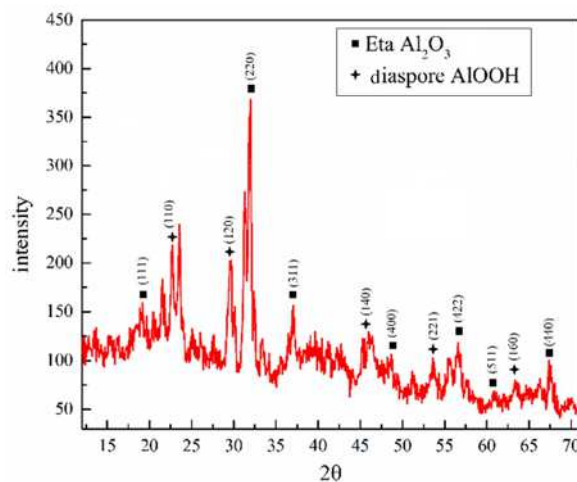


**Fig. 7** XRD patterns of sample 8: 2 min, [NaOH] = 0.6 M, supercritical fluid density = 0.34 g/cm<sup>3</sup>

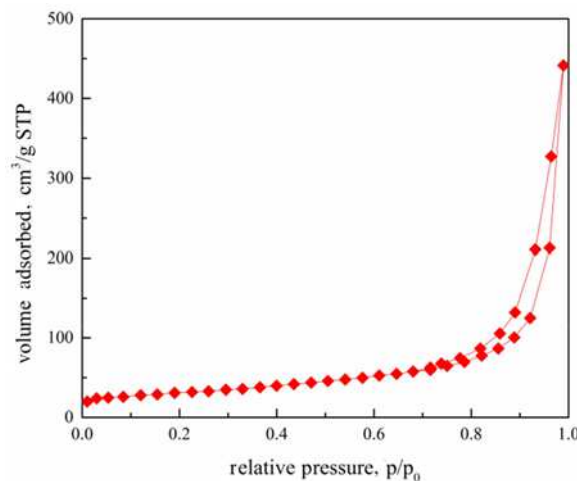


**Fig. 8** N<sub>2</sub> adsorption/desorption isotherms of flower-like η-alumina

polycrystalline can be produced [47]. Herein, due to the huge increment in supersaturation, plates emerged from cores as a result of radial growth (Fig. 6c).

At the density of 0.17 g/cm<sup>3</sup>, η-alumina nanoflakes were formed from diaspore (Fig. 6a). The formation of nanoflake morphology in this situation is triggered by the naturally layered crystal structure of diaspore as the primary source of η-alumina. By raising the density, nucleation happened with high intensity. Owing to intense nucleation, a high number of spherical nuclei created and attached together to form nanosphere aggregates (Fig. 6b). The flower-like particle formation process included two steps. First because of high supersaturation, a high number of initial particles aggregate together to form spherical cores. Second, nanoflakes formed on the surface of these spherical cores (Fig. 6c). This lamellar growth of flower petals is similar to the nanoflake formation at low densities in the present work.

**4. Conclusion:** Eta alumina (η-Al<sub>2</sub>O<sub>3</sub>) powders were rapidly synthesised via a one-step supercritical hydrothermal route at 500°C without calcination for the first time. The synthesis time was reduced to 2 min by taking advantage of the molten salt bath as a rapid heating source. The influential factors of η-Al<sub>2</sub>O<sub>3</sub> synthesis, such as reaction time, the dosage of NaOH and supercritical solution density were determined, and then a mechanism for the

production of flower-like morphology was suggested. It was found that adding NaOH boosts dehydration and oxidation reactions in the synthesis process; so that  $\eta$ -Al<sub>2</sub>O<sub>3</sub> was produced effortlessly at basic pH. At a low density of the supercritical fluid, nanoplates of  $\eta$ -Al<sub>2</sub>O<sub>3</sub> were produced. While by increasing the density, flower-like hierarchical morphology was formed. The flower-like particle precipitation mechanism consists of two steps. The first step is aggregating initial particles to form spherical cores, and then emerging two-dimensional nanopetals on the surface of these cores.

## 5 References

- Levin I., Brandon D.: 'Metastable alumina polymorphs: crystal structures and transition sequences', *J. Am. Ceram. Soc.*, 1998, **81**, pp. 1995–2012
- Roy R., Hill V.G., Osborn E.F.: 'Polymorphs of alumina and gallia', *Ind. Eng. Chem.*, 1953, **45**, pp. 819–820
- Saha D., Deng S.: 'Characteristics of ammonia adsorption on activated alumina', *J. Chem. Eng. Data*, 2010, **55**, pp. 5587–5593
- Kim J., Lee H., Vo H., *ET AL.*: 'Bead-shaped mesoporous alumina adsorbents for adsorption of ammonia', *Materials. (Basel)*, 2020, **13**, p. 1375
- Kasprzyk-Hordern B.: 'Chemistry of alumina, reactions in aqueous solution and its application in water treatment', *Adv. Colloid Interface Sci.*, 2004, **110**, pp. 19–48
- Bishop P.L., Sansoucy G.: 'Fluoride removal from drinking water by fluidized activated alumina adsorption', *J. AWWA*, 1978, **70**, pp. 554–559
- Kasprzyk-Hordern B., Raczky-Stanislawiak U., Świetlik J., *ET AL.*: 'Catalytic ozonation of natural organic matter on alumina', *Appl. Catal., B*, 2006, **62**, pp. 345–358
- Lin T.-F., Wu J.-K.: 'Adsorption of arsenite and arsenate within activated alumina grains: equilibrium and kinetics', *Water Res.*, 2001, **35**, pp. 2049–2057
- Naiya T.K., Bhattacharya A.K., Das S.K.: 'Adsorption of Cd(II) and Pb(II) from aqueous solutions on activated alumina', *J. Colloid Interface Sci.*, 2009, **333**, pp. 14–26
- Tripathy S.S., Bersillon J.-L., Gopal K.: 'Removal of fluoride from drinking water by adsorption onto alum-impregnated activated alumina', *Sep. Purif. Technol.*, 2006, **50**, pp. 310–317
- Ghorai S., Pant K.K.: 'Equilibrium, kinetics and breakthrough studies for adsorption of fluoride on activated alumina', *Sep. Purif. Technol.*, 2005, **42**, pp. 265–271
- Manasip A., Gulari E.: 'Selective CO oxidation over Pt/alumina catalysts for fuel cell applications', *Appl. Catal., B*, 2002, **37**, pp. 17–25
- Shyu J.Z., Otto K., Watkins W.L.H., *ET AL.*: 'Characterization of Pd/ $\gamma$ -alumina catalysts containing ceria', *J. Catal.*, 1988, **114**, pp. 23–33
- Arzamendi G., Campo I., Arguñarena E., *ET AL.*: 'Synthesis of biodiesel with heterogeneous NaOH/alumina catalysts: comparison with homogeneous NaOH', *Chem. Eng. J.*, 2007, **134**, pp. 123–130
- Levin I., Bendersky L.A., Brandon D.G., *ET AL.*: 'Cubic to monoclinic phase transformations in alumina', *Acta Mater.*, 1997, **45**, pp. 3659–3669
- Levin I., Gemming T., Brandon D.G.: 'Some metastable polymorphs and transient stages of transformation in alumina', *Phys. Status Solidi (A)*, 1998, **166**, pp. 197–218
- Andersson J.M.: 'Controlling the Formation and Stability of Alumina Phases', in: Linköping Studies in Science and Technology. Dissertations, Institutionen för fysik, kemi och biologi, 2005
- Lietti L., Forzatti P., Nova I., *ET AL.*: 'NOx storage reduction over Pt-Ba/ $\gamma$ -Al<sub>2</sub>O<sub>3</sub> catalyst', *J. Catal.*, 2001, **204**, pp. 175–191
- Şenol O.İ., Viljava T.R., Krause A.O.I.: 'Hydrodeoxygenation of aliphatic esters on sulphided NiMo/ $\gamma$ -Al<sub>2</sub>O<sub>3</sub> and CoMo/ $\gamma$ -Al<sub>2</sub>O<sub>3</sub> catalyst: the effect of water', *Catal. Today*, 2005, **106**, pp. 186–189
- Goula M.A., Kontou S.K., Tsiakaras P.E.: 'Hydrogen production by ethanol steam reforming over a commercial Pd/ $\gamma$ -Al<sub>2</sub>O<sub>3</sub> catalyst', *Appl. Catal., B*, 2004, **49**, pp. 135–144
- Beuls A., Swalus C., Jacquemin M., *ET AL.*: 'Methanation of CO<sub>2</sub>: further insight into the mechanism over Rh/ $\gamma$ -Al<sub>2</sub>O<sub>3</sub> catalyst', *Appl. Catal., B*, 2012, **113–114**, pp. 2–10
- Chen Y., Hyldtoft J., Jacobsen C.J.H., *ET AL.*: 'NIR FT Raman spectroscopic studies of  $\eta$ -Al<sub>2</sub>O<sub>3</sub> and Mo/ $\eta$ -Al<sub>2</sub>O<sub>3</sub> catalysts', *Spectrochim. Acta, Part A*, 1995, **51**, pp. 2161–2169
- Seyedmonir S.R., Strohmayer D.E., Geoffroy G.L., *ET AL.*: 'Characterization of supported silver catalysts II. Adsorption studies of well-dispersed Ag on  $\eta$ -Al<sub>2</sub>O<sub>3</sub>', *Adsorpt. Sci. Technol.*, 1984, **1**, pp. 253–267
- Jacobsen C.J.H., Topsoe N.Y., Topsoe H., *ET AL.*: 'Quantitative 1H MAS NMR studies of structurally different OH surface groups on  $\eta$ -Al<sub>2</sub>O<sub>3</sub> and mol-/ $\eta$ -Al<sub>2</sub>O<sub>3</sub> catalysts', *J. Catal.*, 1995, **154**, pp. 65–68
- Osman A.I., Meudal J., Laffir F., *ET AL.*: 'Enhanced catalytic activity of Ni on  $\eta$ -Al<sub>2</sub>O<sub>3</sub> and ZSM-5 on addition of ceria zirconia for the partial oxidation of methane', *Appl. Catal., B*, 2017, **212**, pp. 68–79
- Osman A.I., Abu-Dahrieh J.K., Abdelkader A., *ET AL.*: 'Silver-modified  $\eta$ -Al<sub>2</sub>O<sub>3</sub> catalyst for DME production', *J. Phys. Chem. C*, 2017, **121**, pp. 25018–25032
- Kobra N., Yeganeh S., Faezeh Jame C.: 'Nano alumina catalytic applications in organic transformations', *Mini-Rev. Org. Chem.*, 2019, **16**, pp. 102–110
- Ardiyanti A.R., Khromova S.A., Venderbosch R.H., *ET AL.*: 'Catalytic hydrotreatment of fast-pyrolysis oil using non-sulfided bimetallic Ni-Cu catalysts on a  $\delta$ -Al<sub>2</sub>O<sub>3</sub> support', *Appl. Catal., B*, 2012, **117–118**, pp. 105–117
- Opoku-Gyamfi K., Adesina A.A.: 'Kinetic studies of CH<sub>4</sub> oxidation over Pt-NiO/ $\delta$ -Al<sub>2</sub>O<sub>3</sub> in a fluidised bed reactor', *Appl. Catal., A*, 1999, **180**, pp. 113–122
- Marceau E., Lauron-Pernot H., Che M.: 'Influence of the metallic precursor and of the catalytic reaction on the activity and evolution of Pt(Cl)/ $\delta$ -Al<sub>2</sub>O<sub>3</sub> catalysts in the total oxidation of methane', *J. Catal.*, 2001, **197**, pp. 394–405
- Farajimotlagh M., Poursalehi R., Aliofkhaeizaei M.: 'Synthesis mechanisms, optical and structural properties of  $\eta$ -Al<sub>2</sub>O<sub>3</sub> based nanoparticles prepared by DC arc discharge in environmentally friendly liquids', *Ceramics Int.*, 2017, **43**, pp. 7717–7723
- Jacobs G., Ribeiro M.C., Ma W., *ET AL.*: 'Group 11 (Cu, Ag, Au) promotion of 15%Co/Al<sub>2</sub>O<sub>3</sub> Fischer-tropsch synthesis catalysts', *Appl. Catal., A*, 2009, **361**, pp. 137–151
- Li P., Liu J., Nag N., *ET AL.*: 'In situ synthesis and characterization of Ru promoted Co/Al<sub>2</sub>O<sub>3</sub> Fischer-tropsch catalysts', *Appl. Catal., A*, 2006, **307**, pp. 212–221
- Yang Z., Cai W., Zhou J., *ET AL.*: 'Fast, large-scale, and stable preparation of  $\eta$ -Al<sub>2</sub>O<sub>3</sub> microspheres by fully utilizing N, N-dimethylformamide at room temperature', *Ind. Eng. Chem. Res.*, 2020, **59**, pp. 4203–4209
- Sun R., Shen S., Zhang D., *ET AL.*: 'Hydrofining of coal tar light oil to produce high octane gasoline blending components over  $\gamma$ -Al<sub>2</sub>O<sub>3</sub>- and  $\eta$ -Al<sub>2</sub>O<sub>3</sub>-supported catalysts', *Energy Fuels*, 2015, **29**, pp. 7005–7013
- Pradhan J.K., Bhattacharya I.N., Das S.C., *ET AL.*: 'Characterisation of fine polycrystals of metastable  $\eta$ -alumina obtained through a wet chemical precursor synthesis', *Mater. Sci. Eng.: B*, 2000, **77**, pp. 185–192
- Seo C.W., Jung K.D., Lee K.Y., *ET AL.*: 'Influence of structure type of Al<sub>2</sub>O<sub>3</sub> on dehydration of methanol for dimethyl ether synthesis', *Ind. Eng. Chem. Res.*, 2008, **47**, pp. 6573–6578
- Osman A.I., Abu-Dahrieh J.K., Rooney D.W., *ET AL.*: 'Effect of precursor on the performance of alumina for the dehydration of methanol to dimethyl ether', *Appl. Catal., B*, 2012, **127**, pp. 307–315
- Hayashi H., Hakuta Y.: 'Hydrothermal synthesis of metal oxide nanoparticles in supercritical water', *Materials (Basel)*, 2010, **3**, pp. 3794–3817
- Adschiri T., Hakuta Y., Arai K.: 'Hydrothermal synthesis of metal oxide fine particles at supercritical conditions', *Ind. Eng. Chem. Res.*, 2000, **39**, pp. 4901–4907
- Adschiri T., Hakuta Y., Sue K., *ET AL.*: 'Hydrothermal synthesis of metal oxide nanoparticles at supercritical conditions', *J. Nanopart. Res.*, 2001, **3**, pp. 227–235
- Hakuta Y., Hayashi H., Arai K.: 'Fine particle formation using supercritical fluids', *Curr. Opin. Solid State Mater. Sci.*, 2003, **7**, pp. 341–351
- Noguchi T., Matsui K., Islam N.M., *ET AL.*: 'Rapid synthesis of  $\gamma$ -Al<sub>2</sub>O<sub>3</sub> nanoparticles in supercritical water by continuous hydrothermal flow reaction system', *J. Supercrit. Fluids.*, 2008, **46**, pp. 129–136
- Jalouli B., Abbasi A., Musavi Khoei S.M.: 'A comment on: conventional and microwave hydrothermal synthesis and application of functional materials: a review', *Materials (Basel)*, 2019, **12**, p. 3631
- Kolis J.W., Korzenski M.B.: 'The synthesis of transition metal sulfides and sulfo-salt crystals in hydrothermal brines', *MRS Proceedings*, 1996, **453**, p. 35
- Brunner G.: p'Chapter 11 - hydrothermal and supercritical water processing of inorganic substances', in: Brunner G. (Ed.): 'Supercritical fluid science and technology' (Elsevier, Netherlands, 2014), pp. 569–589
- Sunagawa I.: 'Crystals: growth, morphology, and perfection' 2005